INTERNATIONAL JOURNAL
FOR RESEARCH

IN APPLIED SCIENCE & ENGINEERING TECHNOLOGY

www.ijraset.com

Call: ⓒ08813907089 | E-mail ID: ijraset@gmail.com

A Numerical Study on the Influences of Non-Pneumatic Tyre Shape on the Wheel Aerodynamics

M. Z. Soliman[1], A. M. R. El-Baz[2], M. A. Abdel-Aziz[3], N. Abdel-Aziz[4]

[1, 3]Automotive Engineering, Ain-Sham University, Cairo, Egypt
[2] Mechanical Engineering Department, The British University in Egypt, Cairo, Egypt
[4]Mechanical Power Department, Ain-Sham University, Cairo, Egypt

Abstract: In the present work, the aerodynamic characteristics of two different tyre shapes, Slick Tyre (ST) and Non-Pneumatic Tyre (NPT), fitted to a rotating wheel, has been investigated using a CFD approach. The ST wheel has been primarily utilized to examine the adopted numerical model's validity. The ST wheel pressure coefficient (Cp) profile at its central plane (XY) has directly compared with the robust experimental data experienced from the literature. Further assessments on the computationally obtained outcomes such as drag coefficient, separation and stagnation angular locations are performed. Both wheel cases are compared concerning their aerodynamic coefficients and the flow characteristics around the wheel. Besides, for the NPT wheel case, a shape-optimization study changes the wheel side profile's spokes angle (α) is conducted. The dynamic action of wheel rotation is modelled using the Moving Reference Frame (MRF) technique, and the RNG k- ε is utilized as the adopted turbulence model for Averaged Reynolds Navier Stokes equations (RANS). All cases run at 30 m/s upstream velocity to be within the fully developed flow regime (supercritical regime). That is equivalent to 6.8×10^5 Reynolds number based on the wheel diameter as the characteristic length. In general, the overall obtained results give a satisfactory agreement to those measured experimentally. In conclusion, The NPT wheel, compared to the ST wheel, has a dramatic increase in drag force by approximately 31%, while a slightly raised lift force is obtained. The minimized spoke angle came with a beneficial drag reduction, while the applied resistive moment remained relatively high.
Keywords: automotive aerodynamics; wheel aerodynamics, tyre CFD; rotating wheel dynamics; MRF wheel simulation; airless tyre aerodynamics, non-pneumatic tyre aerodynamics.

I. INTRODUCTION

Recently, the vehicle body shape has become well-optimized, and the wheel aerodynamics reveals a poorly understood part that might make significance. In fact, the wheel primitive geometry is cylindrical, so from the aerodynamic perspective, the wheel represents a blunt body that provides increments in base drag. Therefore, the wheel seems to be an influential vehicle part, especially for the applications in which wheels are entirely exposed to the airflow, such as commercial high sided vehicles; Trucks and semi-trailers. Improving the aerodynamic characteristics of these particular applications is likely to have a substantial impact on economics. However, fitting the new trendy NPT wheels to these applications ensures higher safety levels; their side profile is expected to have a dramatic drag increment since hard textures are comprised.

In general, wheel aerodynamics characteristics has a complex flow field accompanied with dynamic transient effects due to the additional tread features and rim details. In 1967, Morelli **[Error! Reference source not found.** started to experimentally measure the aerodynamic coefficient of an isolated racing car wheel. The rotating wheel was not touching the stationary ground, where a minimal gap was maintained. He found that the rotating wheel can produce a 10% higher drag coefficient than the stationary one. Also, the rotating wheel has generally a negative lift value. Other subsequent attempts to sufficiently seal the wheel-ground gaps using paper sheets and brushes have been made by Stapleford and Carr **[Error! Reference source not found.** and Cogotti **[Error! Reference source not found.**. They emphasized that the rotating wheel has a positive lift and Morelli's setup has improper wheel-ground modelling. Fackrell **[Error! Reference source not found.** measured the surface pressure profile, and a dramatic pressure rise (Cp > 2) located at the front of the contact patch has obtained. This phenomenon has been argued as wheel rotation's dynamic action squeezes the flow approaching this region and causes a pressurized flow. A series of comprehensive studies on visualizing the flow field around the isolated wheel has been done at the advent of the current century. Knowles et al. **[Error! Reference source not found.** utilized the Laser Doppler Anemometry technique (LDA) over scanning four downstream planes. Two primary streamwise vortices gathered in a reversed-T shaped downstream are developed; one pair is induced from the wheel top separation, and another is shed from the wheel sidewall near the ground.

The last appears firmer and further extended downstream. Other majorities use Particle Image Velocimetry (PIV) to understand further the dynamics of wheel wake, such as Mears et al. [**Error! Reference source not found.**, Van Den Berg [

Mears AP, Crossland SC, Dominy RG. An investigation into the flow-field about an exposed racing wheel. SAE Technical Paper; 2004 Mar 8. , Heyder-Bruckner [

Van den Berg MA. Aerodynamic interaction of an inverted wing with a rotating wheel (Doctoral dissertation, University of Southampton). , Sprot et al. [

Heyder-Bruckner J. The aerodynamics of an inverted wing and a rotating wheel in ground effect (Doctoral dissertation, University of Southampton). , Croner et al. [**Error! Reference source not found.**, and recently Haag et al.'s [

Croner E, Bézard H, Sicot C, Mothay G. Aerodynamic characterization of the wake of an isolated rolling wheel. International journal of heat and fluid flow. 2013 Oct 1;43:233-43. and Rajaratnam and Walker [**Error! Reference source not found.**. Their experiments precisely matched the wake structure results obtained by Knowles et al. [**Error! Reference source not found.**. Besides, a transient shedding behaviour is commonly observed at the upper and lower streamwise vortices but not similar to Von Karmen vortex street. Other valuable outcomes demonstrated faster dissipation of the lower-outward vortex due to the counter hub flow when the detailed rim is considered. In the computational studies, strong recommendations about using the Moving Reference frame (MRF) technique is a promising economical alternative to Sliding Mesh (SM) to simulate the dynamic rotational effects of rim spokes. In addition, the Moving Wall boundary condition (MW) seemed to lack the correct in-hub flow due to its complicity and accompanied unsteadiness effects, as frequently concluded by Yu et al. [

Rajaratnam E, Walker D. Experimental and computational study of the flow around a stationary and rotating isolated wheel and the influence of a moving ground plane. SAE Technical Paper; 2019 Apr 2., Hagg et al.[

Croner E, Bézard H, Sicot C, Mothay G. Aerodynamic characterization of the wake of an isolated rolling wheel. International journal of heat and fluid flow. 2013 Oct 1;43:233-43. , Hobeika and Sebben [

Yu X, Jia Q, Bao D, Yang Z. A comparative study of different wheel rotating simulation methods in automotive aerodynamics. SAE Technical Paper; 2018 Apr 3. , and Lewis et al.[

Hobeika T, Sebben S. CFD investigation on wheel rotation modelling. Journal of Wind Engineering and Industrial Aerodynamics. 2018 Mar 1;174:241-51. .

Regarding the NPT wheels, some relevant articles that computationally argued their aerodynamic characteristics, but only the moving wall boundary condition (MW) approach is the only considered. The MW approach is not a particular modelling choice for NPT wheels due to its lack of presenting the additional angular momentum of spokes rotation. However, so respected outcomes which give a prior understanding of NPT flow physics is obtained. Heo et al. [

Lewis R, Cross M, Ludlow D. The influence of rotating wheels on the external aerodynamic performance of a vehicle. InThe International Vehicle Aerodynamics Conference 2014 Nov 12 (pp. 161-173). Woodhead Publishing. [

Heo H, Ju J, Kim DM, Rhie S. A study on the aerodynamic drag of a non-pneumatic tire. InInternational Design Engineering Technical Conferences and Computers and Information in Engineering Conference 2012 Aug 12 (Vol. 45059, pp. 517-521). American Society of Mechanical Engineers. utilized the RNG k-SRANS solver to investigate the near-wake structure of a wedge-shaped NPT wheel. He concluded that side spokes could greatly intricate the flow pattern at the side surface, causing significant drag rise.

Li et al. [

Heo H, Ju J, Kim DM, Kim H. A computational study of the flow around an isolated non-pneumatic tire. SAE International Journal of Passenger Cars-Mechanical Systems. 2014 May 10;7(2014-01-9123):405-12. added that longer and thicker spokes had been shown to lower the wheel's aerodynamic coefficients significantly. They also created a model of a competitive vehicle with four NPT wheels. It found that the high leverage of generated turbulence from the wheels produces an 8.2% increase in drag over the ST scenario. Bhatia et al. [

Li H, Xu Y, Si C, Yang Y. A research on aerodynamic characteristics of non-pneumatic tire. Mechanics & Industry. 2021;22:27. focused on a comparable NPT wedge type and another basic hexagonal honeycomb form.

There was no significant difference in drag coefficient between the two different types; however, the honeycomb shape had a slightly lower lift coefficient. He came to the conclusion that the SST k- blended model might outperform the k- model near the spokes. Amongst the researchers' promising contributions, an interesting parameter of wheel moment coefficient CM is rarely considered. Soliman et al. [

Bhatia D, KR P, Ponangi BR, Athadkar M, Dsouza CV. CFD study of aerodynamic performance of non-pneumatic tyre with hexagonal spokes. Proceedings of the Institution of Mechanical Engineers, Part D: Journal of Automobile Engineering. 2021 May 3:09544070211013124. reported that the parameter strongly impacts the net wheel drag where the exposed wheel rotates against the upstream flow direction.

That leads to higher shear stress at the wheel top boundary layer resulting in an applied resistive torque. The NPT spokes have expected to dramatically raise the value of the applied resistive toque since they have intricate surface textures. Therefore, studying the aerodynamic characteristics of the ST and NPT wheel types has been argued in the current work. Moreover, using the MRF to realistically expressing the spokes rotational effects in NPT wheel model instead of MW is extremely considered. Further parametric study on changing the NPT wheel spokes angles is carried out.

II.   WHEEL MODEL

A. ST Wheel Geometry

International Journal for Research in Applied Science & Engineering Technology (IJRASET)
ISSN: 2321-9653; IC Value: 45.98; SJ Impact Factor: 7.538
Volume 10 Issue II Feb 2022- Available at www.ijraset.com

A half-scaled 3D CAD drawing of an ST wheel is typically drawn to that used in Van Den Berg's [

Mears AP, Crossland SC, Dominy RG. An investigation into the flow-field about an exposed racing wheel. SAE Technical Paper; 2004 Mar 8. experimental setup to verify the present adopted computational model. Figure 1Figure *1*. The 3D construction drawing of typical ST wheel (all dimensions in mm). shows the detailed dimensions of the constructed 3D wheel comprising an evenly spaced four circumferential grooves. The wheel ground contact is modelled using the plint technique to sufficiently avoid the strongly skewed grids at this critical region. That approach is often applied through most computational attempts in the literature [

Mears AP, Crossland SC, Dominy RG. An investigation into the flow-field about an exposed racing wheel. SAE Technical Paper; 2004 Mar 8. [

Van den Berg MA. Aerodynamic interaction of an inverted wing with a rotating wheel (Doctoral dissertation, University of Southampton). [

Heyder-Bruckner J. The aerodynamics of an inverted wing and a rotating wheel in ground effect (Doctoral dissertation, University of Southampton).

Yu X, Jia Q, Bao D, Yang Z. A comparative study of different wheel rotating simulation methods in automotive aerodynamics. SAE Technical Paper; 2018 Apr 3.], where it was a promising solution for that issue.

B. NPT Wheel Geometry
A similar ST wheel CAD model is utilized with a sidewall modification, where 20 evenly spaced spokes were added to meet the typical airless tyre shape, as shown in Figure 2 . Further adjustment to the rounded side profile since standard NPT wheels customarily have a smaller radius. Figure 2 also shows the detailed dimensions of NPT wheel geometry. Since rims are intensively interacting with the flow field near wheel sides, the rim detail kept eliminated as in the ST wheel model. Rim is redeemed by a flattened cover to allow individually investigating the effect of the NPT spokes. The longitudinal wheel grooves are omitted to simplify the NPT model.

The plint approach has also developed at the contact patch region to avoid the undesirable sharp corners that intuitively formed from the wheel-ground contact. A parametric study of varying the supporting spokes angle (α), indicated in Figure 2, is assigned to optimizing the wheel shape.

C. Computational domain
In all the present cases, the surrounding wheel domain is constructed as 6 times the wheel diameter (6D) square cross-sectional area with a total length of 18D, as shown in Figure 3 . According to the overall wheel dimensions, these settled dimensional ratios assign a blockage ratio of 6.2%, which is sufficiently beneath the maximum limitation **[Error! Reference source not found. [Error! Reference source not found. [**

Mears AP, Crossland SC, Dominy RG. An investigation into the flow-field about an exposed racing wheel. SAE Technical Paper; 2004 Mar 8. . The wheel body is placed behind the inlet boundary so that a 5D upstream length is allocated.

Whilst the rest of the domain length, 13D, is dedicated for the downstream. This division ratio is so necessary to capture the correct highly-induced turbulence downstream.

It should be noted that the computational domain undergoes some splitting processes to fulfil the meshing optimization demands. The computational domain has bisected at the wheel middle plane since wheel geometries and its flow patterns are symmetric. This technique dramatically reduces the computational time by allowing only the modelling of half of the computational domain. Another necessary splitting has developed by separating the wheel surrounding zone from the modelled half of the computational domain.

That came with the benefit of allowing the grid to be much denser near the wheel, where tremendous flow characteristics are expected. At the rest of the computational domain, the grid has remained larger since airflow has neglected variations. Also, one more splitting is devoted to utilizing the MRF approach, where a particular surrounding zone to the wheel is needed to augment the additional angular momentum to the flow governing equations. An inflated wheel shape with a diametrical upward offset of 0.01D from its surface is prepared for that purpose.
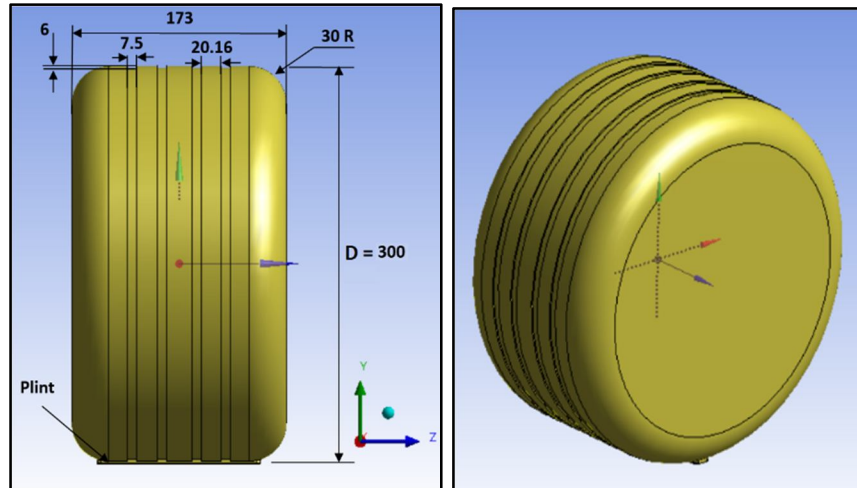
Figure 1. The 3D construction drawing of typical ST wheel (all dimensions in mm).
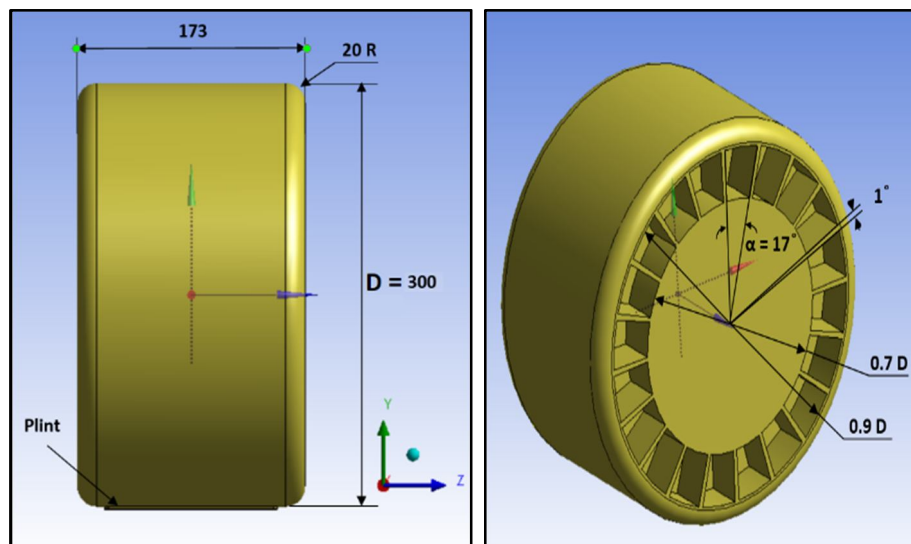

Figure 2. The 3D construction drawing of typical NPT wheel at (α) = 17 degrees (all dimensions in mm).
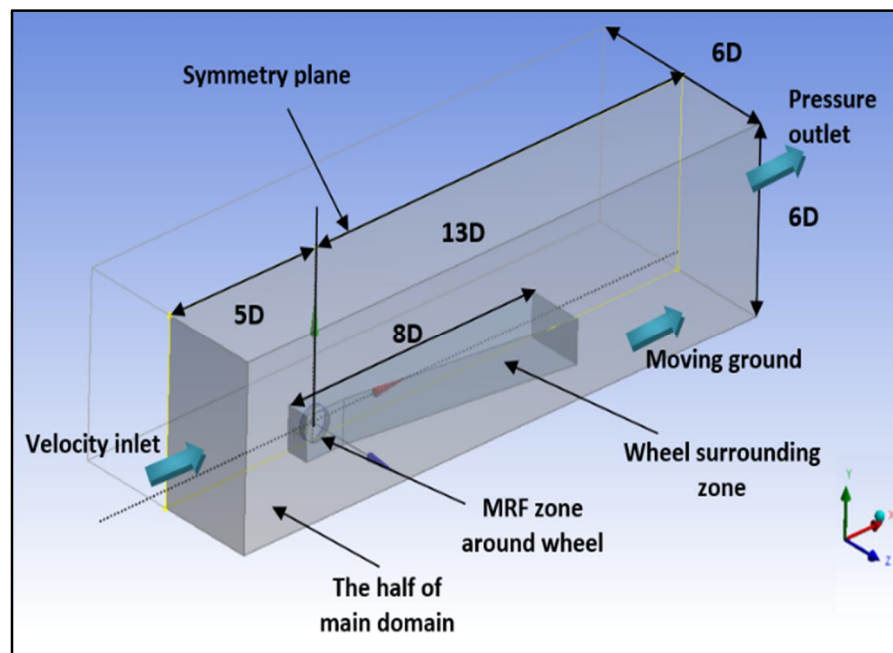
Figure 3. The schematics of the Computational domain.

III. BOUNDARY CONDITIONS

To possibly close the domain boundary conditions to the actual far-field conditions, velocity inlet and pressure outlet choice are the most appropriate conditions where the known upstream velocity and atmospheric pressures can be defined. A normal velocity inlet condition of 30 m/s (Re = 6.8 ×105) based on the wheel diameter (D) is set to the inlet flow surface, as shown in Figure 3. The turbulence intensity is limited to 0.3% as measured experimentally, and the hydraulic diameter of 1D is defined for the upstream turbulence characteristics. An atmospheric pressure condition is defined for the outlet flow surface. The ground surface is specified as a moving wall with the same upstream velocity magnitude and direction, where a non-slip condition is applied. To approach the sides and top situations precisely, they are assumed to be symmetrical in which zero-shear stress is applied to the bounded flow. The wheel surface has considered as a non-rough wall with a non-slip condition. The MRF zone, including the wheel surface, is defined as a moving zone with a rotational velocity of $\omega = 193.7$ rad/s.

IV. MESH GENERATION

The computational domain is primarily discretized into finite volumes using an unstructured tetrahedron grid throughout the current work, as shown in Figure 4. This grid type is often used for complicated 3D geometries with desired grid quality levels. Due to the limited computational resources, a strict grid optimization process was necessary while generating the domain grides. Besides the domain splitting operations done on geometry, another option of utilizing a non-equilibrium near-wall function approach is applied instead of fully resolve the turbulent viscous sublayer. This solving technique allows near-wall grids to be relatively larger than those used with the fully resolving option. The first layer thickness ($2y$) was started by 2 mm and sequentially re-adjusted until it reached the optimal value of 0.65 mm, where Y^+ values have kept within 25-350, where:

$$Y^+ = y \left(\left(\sqrt{\tau_w/\rho} \right)/v \right) \qquad (1)$$

Where, τ_w is the applied shear stress at a specific point over the wheel surface and v is the air kinematic viscosity. Figure 5 shows the obtained Y^+ values over the entire ST wheel surface, which have ranged between 25 to 350. Furthermore, a grid sensitivity study is implemented on the total grid count. The optimal grid count is received when sufficient stability levels in the aerodynamic coefficients are detected. Six different grid counts are examined, and as shown in Figure 6, the optimal grid count is around 6 million grids which are generalized for all modelled cases.
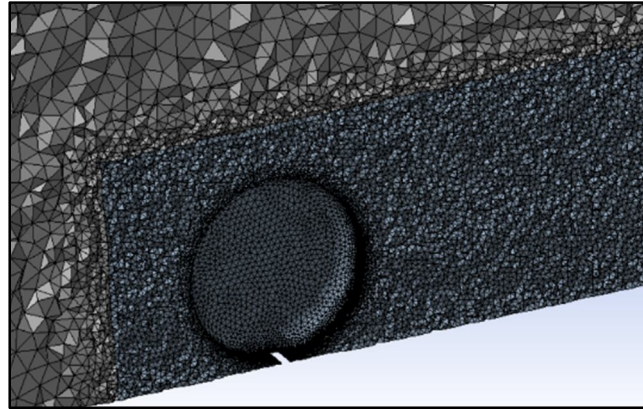
Figure 4. The distribution of the unstructured tetrahedral grid around the ST wheel showing the utilized coarse grids over the free-stream zone and the finer ones over the wheel surrounding zone.
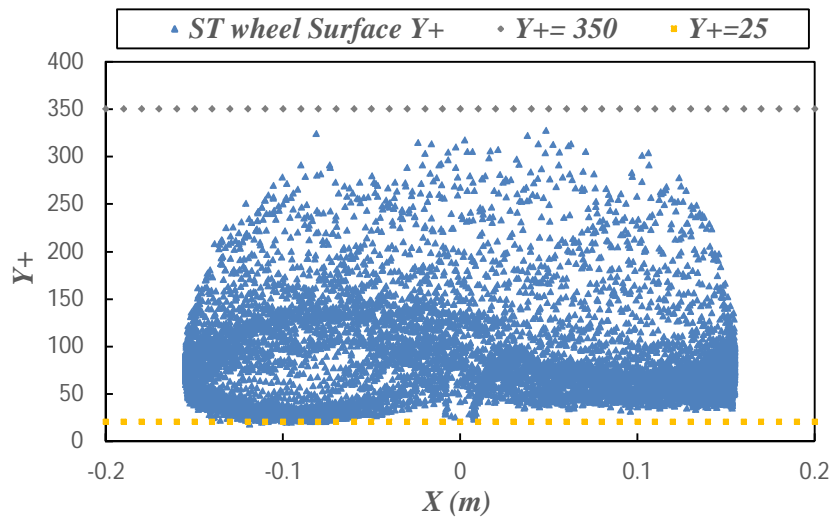

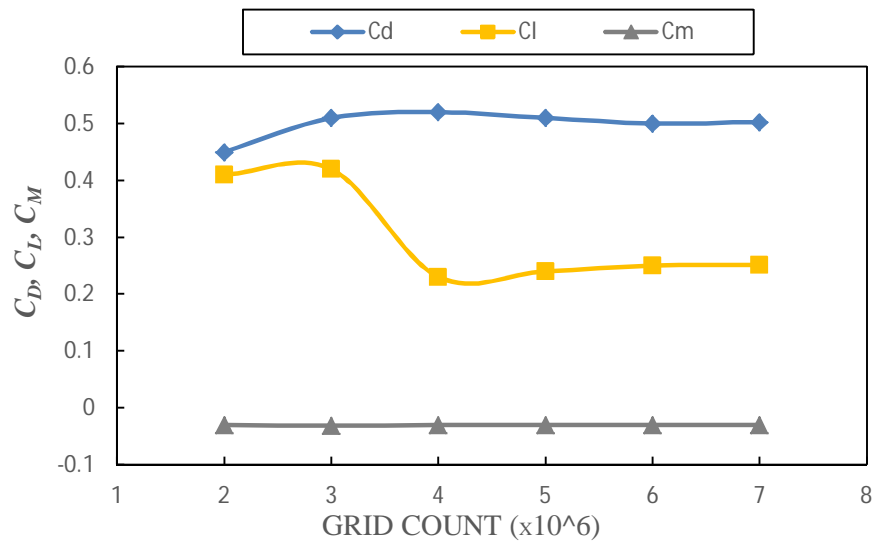Figure 5. The obtained nodal Y+ values of the entire ST wheel surface.

Figure 6. Mesh independence test over the ST wheel aerodynamic coefficients.

International Journal for Research in Applied Science & Engineering Technology (IJRASET)
ISSN: 2321-9653; IC Value: 45.98; SJ Impact Factor: 7.538
Volume 10 Issue II Feb 2022- Available at www.ijraset.com

V. GOVERNING EQUATIONS AND TURBULENCE MODEL

In the present study, all numerical models are solved using ANSYS Fluent software. The governing equations of incompressible flow are solved in the implicit form with a segregated criterion. A SIMPLEC scheme is applied for the coupling between the pressure and velocity dependent-variables. A Second-order discretization scheme is assigned for momentum and turbulent scalar quantities. As reviewed in the literature, K-ε steady RANS is a so accurate and well-verified turbulence model for wheel aerodynamic studies, especially for obtaining surface pressure and force coefficients. This promising turbulence model is utilized and augmented with standard near-wall treatment for viscous sublayer modelling. The flow governing mass and momentum conservation equations have stated as:

$$\nabla \cdot (\rho \bar{v}) = 0 \tag{2}$$

$$\partial/\partial t (\rho \bar{v}) + \nabla \cdot (\rho \bar{v}\bar{v}) = -\nabla p + \nabla \cdot (\bar{\bar{\tau}}) + \rho \bar{g} \tag{3}$$

Where p is the static pressure, $\bar{\bar{\tau}}$ is the stress tensor given by [24]:

$$\bar{\bar{\tau}} = \mu[(\nabla \bar{v} + \nabla \bar{v}^T) - \frac{2}{3} \nabla \cdot \bar{v}I] \tag{4}$$

Where μ is the molecular viscosity, I is the unit tensor. Equation 4 and 5 are ensemble-averaged in cartesian form as [24]:

$$\partial/\partial x_i (\rho u_i) = 0 \tag{5}$$

$$\partial/\partial t (\rho u_i) + \partial/\partial x_j (\rho u_i u_j) = -\partial p/\partial x_i + \partial/\partial x_j \left[\mu \left(\partial u_i/\partial x_j + \partial u_j/\partial x_i - \frac{2}{3} \delta_{ij} \partial u_i/\partial x_l \right) \right] + \partial/\partial x_j (-\rho \overline{u_i' u_j'})$$

$$\tag{6}$$

The term $-\rho \overline{u_i' u_j'}$ in equation (6) is modelled by the adopted turbulence model to close it. On the other hand, for the rotating zone in which the MRF approach is applied, further velocity terms were augmented in the acceleration terms of the momentum equations by the following formulas:

$$\overrightarrow{v_r} = \vec{v} - \overrightarrow{u_r} \tag{7}$$

Where,

$$\overrightarrow{u_r} = \vec{\omega} \times \vec{r} \tag{8}$$

Where, $\overrightarrow{v_r}$ is the relative velocity (the velocity viewed from the rotating frame), $\vec{v}$ is the absolute velocity (the velocity viewed from the stationary frame), $\overrightarrow{u_r}$ is the "whirl" velocity (the velocity due to the moving frame), ω is the rotating frame angular velocity, and $\vec{r}$ is a position vector from the origin of the rotating frame

Soliman MZ, El-Baz AR, Abdel-Aziz MA, Abdel-Aziz N, Sugar-Gabor O. Numerical investigation of the effect of tread pattern on rotating wheel aerodynamics. International Journal of Automotive and Mechanical Engineering. 2020;17(4):8234-45.].

Based on the experienced complex flow field around the 3D wheel, the model undergoes stringent solving steps to ensure sufficient stability levels in convergence. The under-relaxation factors are valued at around 0.25 for pressure and 0.5 for both momentum variables and turbulence quantities. The solution variables start with the initial values defined at the inlet boundary conditions. The solver has initiated using a simple one-equation turbulence model to avoid the hard convergence at the beginning of the run. After approximately 500 iterations, the solver has shifted to the k- ε model, where a sufficient stability level is detected. The solution is determined to terminate when the residuals of all flow variables reach 10^{-4}, and a confident stability level for force coefficients of ±1% variations is monitored. Both conditions were occurred after around 10000 iterations.

VI. RESULTS AND DISCUSSION

This section gathered all computationally obtained outcomes in a comparison form to assess the difference in aerodynamic characteristics between both ST and NPT wheel cases. The pressure profiles over the wheel surface, the forces and moment coefficients, and some captured figures of pressure contours have clearly discussed. Further argument focusing on obtaining the coefficient of the moment for both cases, as the novelty contribution to NPT wheel studies, is included. It should be noted that all these obtained parameters are mainly computed based on the following coefficients formula:

$$C_p = \frac{2(p - p_\infty)}{\rho U_\infty^2} \tag{9}$$

$$C_D = \frac{2F_D}{\rho A_f U_\infty^2} \qquad (10)$$

$$C_L = \frac{2F_L}{\rho A_f U_\infty^2} \qquad (11)$$

$$C_M = \frac{2T_R}{\rho R A_f U_\infty^2} \qquad (12)$$

Where p is the local value of static pressure, ρ is the air density, and U_∞ and p_∞ denotes the velocity and pressure values at the upstream, respectively. F_D and F_L are the wheel aerodynamic applied drag and lift forces, respectively. T_R is the net aerodynamic moment acting on the wheel, R is the wheel radius, and A_f is the wheel frontal area.

A. Validation Case

Amongst the wheel results in the literature that most describes the characteristic of flow around the wheel, the circumferential pressure profile over the wheel's central plane (xy) is the interesting one and often measured. Van Den Berg's [Mears AP, Crossland SC, Dominy RG. An investigation into the flow-field about an exposed racing wheel. SAE Technical Paper; 2004 Mar 8. pressure profile has been captured using advanced measuring techniques that are pretty accurate with high response. Therefore, his experimental pressure profile is recruited as the robust reference for examining the current wheel model. However, RNG k- ε used for steady RANS is a promising model that showed so-compatible outcomes over the wheel studies in the literature; an extra validation case has dictated to examine the consistency of the used MRF technique. As shown in Figure 8, the obtained results from the simulation show a reasonable agreement, where only slight deviations are generally detected. Both contact patch pressure spikes ($\varphi = 85°$, φ =95°), A localized inaccuracy reached nearly 25% error has monitored. Based on the mesh sensitivity study, it experienced that both lacks similarity at the contact patch are firmly dependent on the grid density developed at this region. The limitations in the utilized computational resources allow these discrepancies to be minimized to the values obtained in Figure 7. Since deducing forces coefficients are the core of this study and the contact patch spikes are localized at only two points, their influence on the net integrated pressure profile is insignificant. That is proved in Table 1, where a direct comparison between the computed force coefficients and the experimentally measured by Van Den Berg [Mears AP, Crossland SC, Dominy RG. An investigation into the flow-field about an exposed racing wheel. SAE Technical Paper; 2004 Mar 8. is reviewed. Other interesting aspects, such as stagnation and separation angles, are also examined. The values are near-similar and show that using MRF with RNG k- ε used for steady RANS is a so-consistence computational model and can be generalized throughout this study.
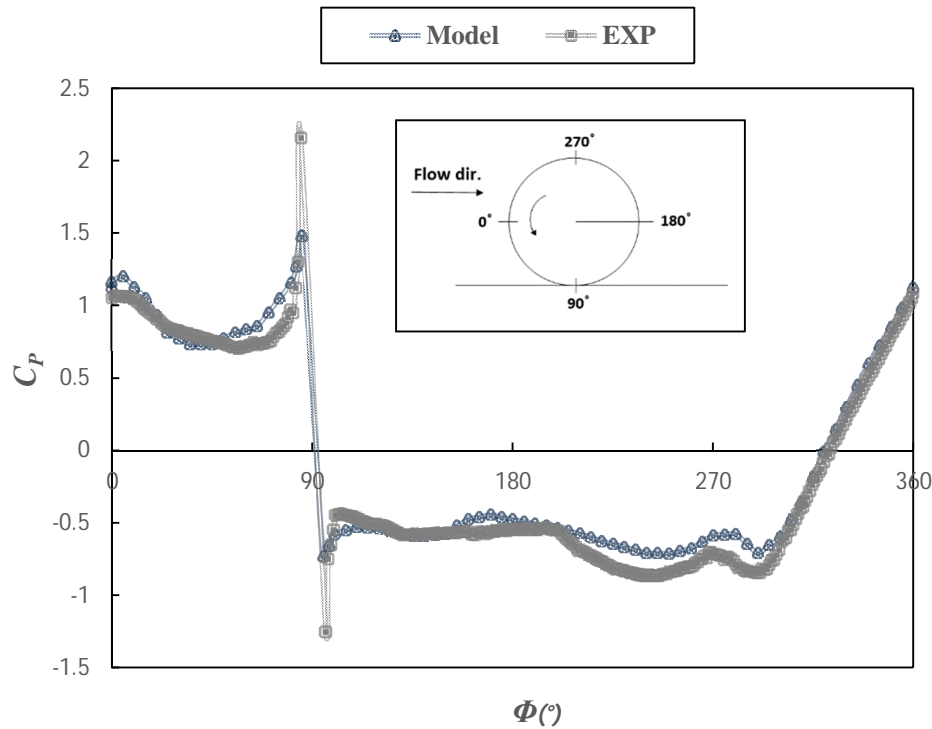
Figure 7. Comparison between the computational pressure coefficient Cp values over ST wheel circumference at (xy) plane and the experimental one done by Van Den Berg [

Mears AP, Crossland SC, Dominy RG. An investigation into the flow-field about an exposed racing wheel. SAE Technical Paper; 2004 Mar 8. .

Table 1. Comparison between the computational and experimental quantitative values.

Method	C_D	C_L	φ Separation	φ Stagnation	Cp_{min}	Cp_{max}
Exp [						
Mears AP, Crossland SC, Dominy RG. An investigation into the flow-field about an exposed racing wheel. SAE Technical Paper; 2004 Mar 8.	0.62	---	275°	6.5°	-1.25	2.16
CFD	0.58	0.60	275°	5.8°	- 0.75	1.49

B. NPT Wheel

The NPT wheel compared to those wheel to clearly spokes' effect. Figure obtained pressure profile at the (xy) for both cases. negative pressure region (φ = 90° - wheel are monitored.

model's results are obtained for the ST understand the side 8 compares the circumferential wheel middle plane Distinct lower values in the wake 225°) for the NPT Besides, a higher

peak in the negative pressure values in the separation region (φ = 225°-270°) is also observed. These variations lead to significantly lower the base drag and increase the lift force.

Table 2Table *1* shows the computed drag, lift, and moment coefficients for both wheel cases, which indicates an inverse trend to that deduced from the pressure profile, where the drag force is dramatically increased. That can be comprehended while observing the sidewall pressure profile, where intensive variations are captured in Figure 9. The NPT spokes induce drastic pressure fluctuations. Since the spokes rotating against the approaching flow, a highly stagnate region is allocated at the spokes heads from φ = 120º to 250º, namely the critical region. As shown in Figure 9, the amplitude at the spokes heads reaches around 1.7, which indicates that the flow acquires additional potential. Figure 10 exhibits the pressure contours over the NPT wheel, evidencing the stagnation ahead of the spokes. The gaps between the NPT spokes are subjected to high-pressure values at the critical region, resulting in an increased drag coefficient. Table 2 also exhibits drag and lift comparison with the recent results in literature, which demonstrate higher drag value for Bhatia et al. [

Li H, Xu Y, Si C, Yang Y. A research on aerodynamic characteristics of non-pneumatic tire. Mechanics & Industry. 2021;22:27., while the lift is close. That indicates the remarkably improvements in the drag results through realistically expressing the rotational dynamics effects using MRF instead of MW. That can be evidenced by the prescribed Fackrell's [Error! Reference source not found. conclusion that the effect of wheel rotation can reduce the darg by around 15% compared to the staionary case, in case of ST wheel, which is expected to be higher for the NPT one.

Further observation in Figure 10 indicates high pressure-differences ΔCp that are applied across the side spokes, which is the main reason for increasing the negative moment coefficient. The moment coefficient of NPT wheel at a designed spacing angle of 17º reaches -0.33 whilst the ST wheel moment coefficient is -0.031 since its side profile is smooth and the viscous friction is only the dominant factor. That came in a friendly way to Soliman et al's [

Bhatia D, KR P, Ponangi BR, Athadkar M, Dsouza CV. CFD study of aerodynamic performance of non-pneumatic tyre with hexagonal spokes. Proceedings of the Institution of Mechanical Engineers, Part D: Journal of Automobile Engineering. 2021 May 3:09544070211013124. suggestions about the highly induced resistive torque.

Table 2. the computed aerodynamic coefficients of ST and NPT (α=17°) wheels

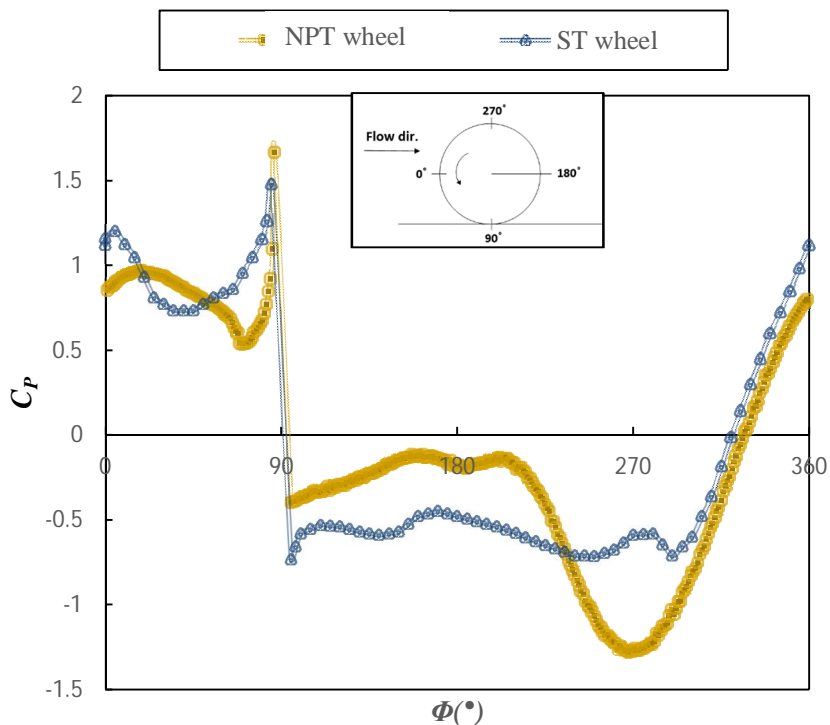| Coef.	ST (present work)	NPT (present work)	NPT wheel Bhatia et al. [
			Li **H, Xu Y, Si C, Yang Y. A research on aerodynamic characteristics of non-pneumatic tire. Mechanics & Industry. 2021;22:27.**
C_D	0.58	0.76	0.993
C_L	0.60	0.67	0.684
C_M	-0.031	-0.33	-

Figure 8. The Circumferential coefficient of pressure profile at the wheel (xy) middle plane of both cases ST and NPT (α=17°) wheels.
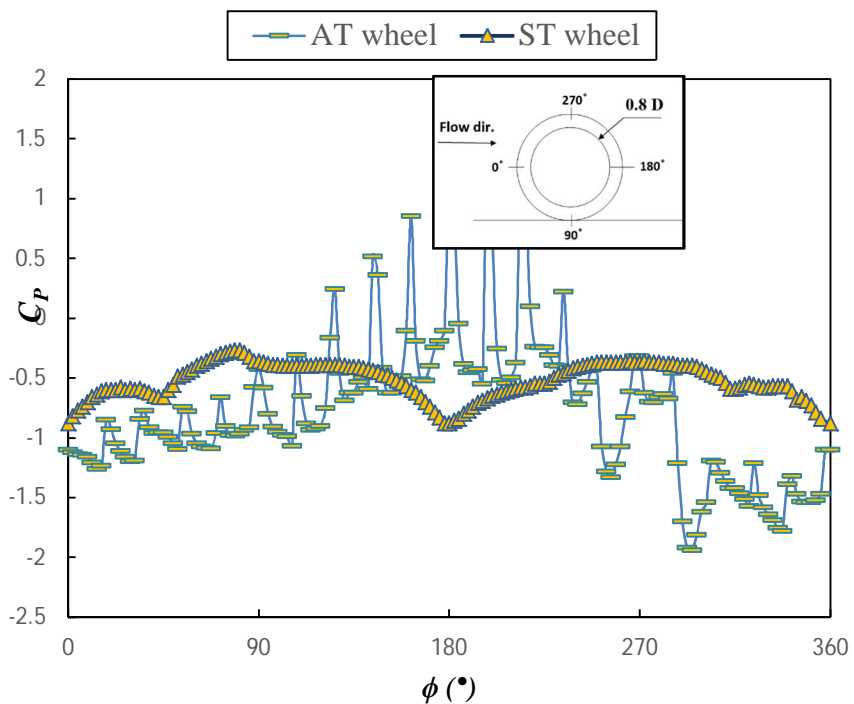

Figure 9. The pressure coefficient profile of the wheel side surface along a circular path of 0.8D diameter for both cases of ST and NPT (α=17°) wheels.
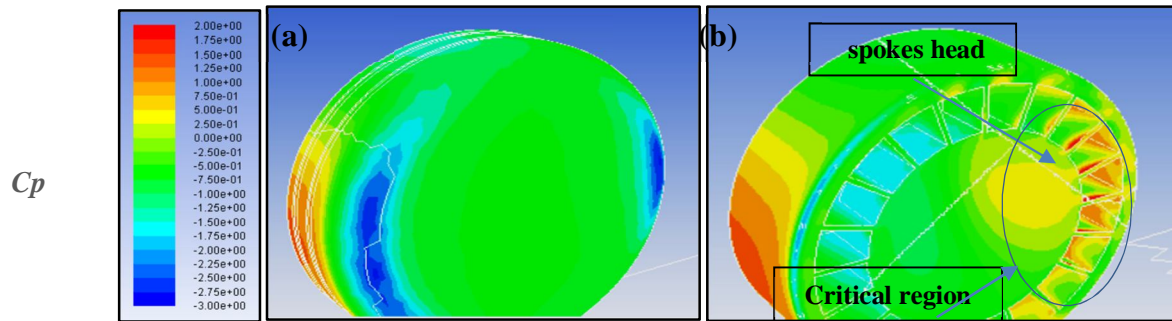
Figure 10. Coefficient of pressure contours at the wheel side of (a) ST wheel and (b) AT (α=17°) wheel.

C. Effect of AT Spacing Angles (α)

This section presents a parametric study investigating the influences of minimizing the NPT wheel's spokes spacing angle (α) on the wheel aerodynamic performance. Five spokes' angles are examined starting from the typical model of α=17° and proceeding by minimizing (α) to 14°, 11°,8°,5°. For a sensible variance, a straight comparison is argued between the two extreme spokes angles, 17° and 5°, for circumferential and side pressure profile, respectively. Figure 11 shows that the circumferential pressure profile of the 5° model has marginal deviations from that of 17°, which individually cause insignificance changes to the aerodynamic coefficients.

Figure 12 indicates obvious variances in the amplitude values of fluctuated pressure for both cases, where at ϕ=200°, the Cp maximum value hits 1.7 for the 17° model, while it just reaches the unity for the 5° ones. The pressure amplitude at the critical region becomes lower as the spacing angle decreases, which causes a dramatic reduction in the drag coefficient. Furthermore, the number of NPT wheel spokes (n) in the 5° model is much more than the 17° one, which causes a decrease in the spoke's gaps that are subjected to the highest-pressure values, hence drag drops. Figure 13 demonstrates the computed drag coefficient values of the five examined spokes angles, which shows that as spacing angles decrease, the drag force drops. That emphasizes Li et al.'s [Heo H, Ju J, Kim DM, Kim H. A computational study of the flow around an isolated non-pneumatic tire. SAE International Journal of Passenger Cars-Mechanical Systems. 2014 May 10;7(2014-01-9123):405-12. conclusion about the thicker spokes (lower gaps area) shows remarkable lesser drag. The drag coefficient is dependent on two multiplied variables; the pressure amplitude and n, which is why the drag curve is exponential.

Figure 12 provides further observations that the pressure differences across the spokes of the 5° model are less than those obtained for 17°. As a result, that drop in pressure differences reduces both the applied negative lift and the moment coefficient. Otherwise, the number of spokes (n) in the 5° model subjected to these tremendous variations become much more than in the 17° one, which influences by increasing both lift and moment coefficients. As shown in Figure 12, as the spacing angles decrease, the net applied lift rises, and the moment drops. In conclusion, descendent ΔCp dominantly impact the negative lift force and moment than the number of spokes. In principle, the lift and moment are strongly governed by two multiplied factors, the descendent ΔCp and the increased (n), which eventually causing slight variations in their values compared to the drag. Figure 14 depicts the averaged pressure coefficient contours distributed over the NPT wheel surface at various spacing angles. it emphasizes the depression in pressure amplitude values in the critical region, as the spokes become closer to each other.
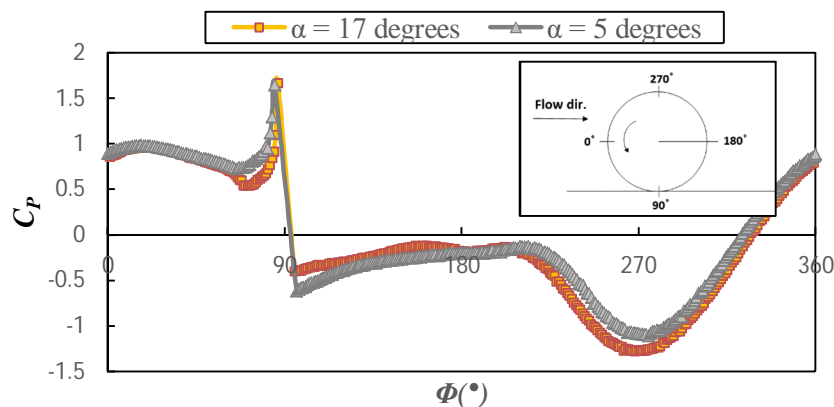
Figure 11. Circumferential coefficient of pressure profile at the wheel (xy) middle plane of both cases AT (α=17°) and NPT (α=5°) wheels.
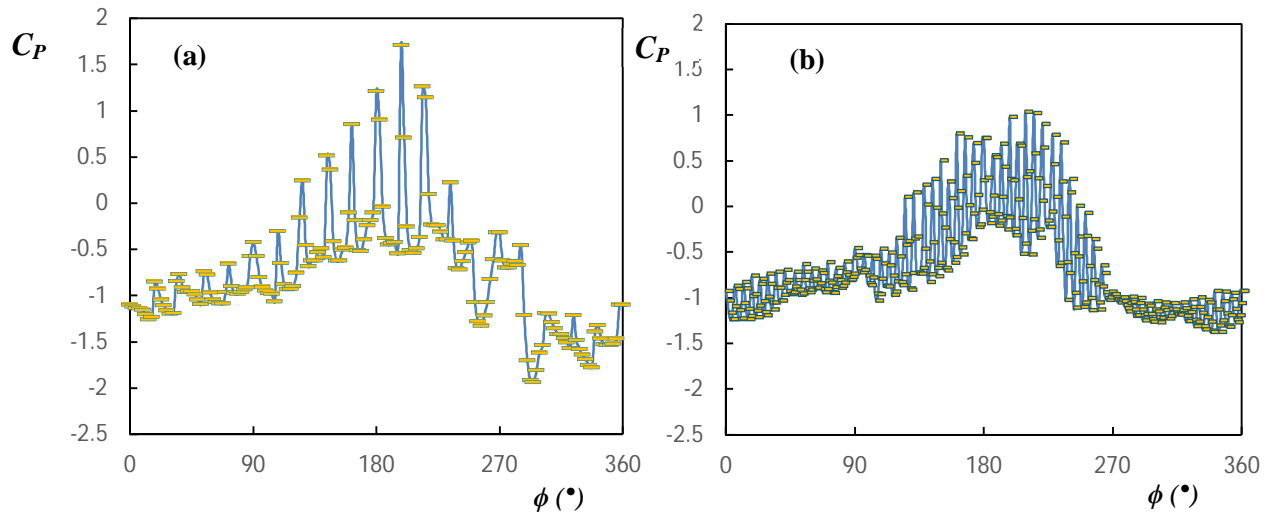

Figure 12. The pressure coefficient profile of the wheel side surface along a circular pass of 0.8D diameter for both cases of (a) NPT (α=17°) and (b) NPT (α=5°) models.
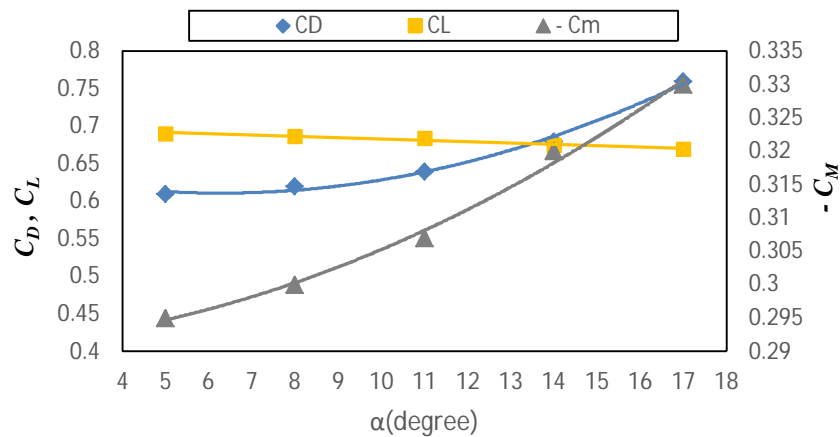

Figure 13. The values of the drag, lift, and moment coefficients at various spokes angles (α) for NPT wheel models.
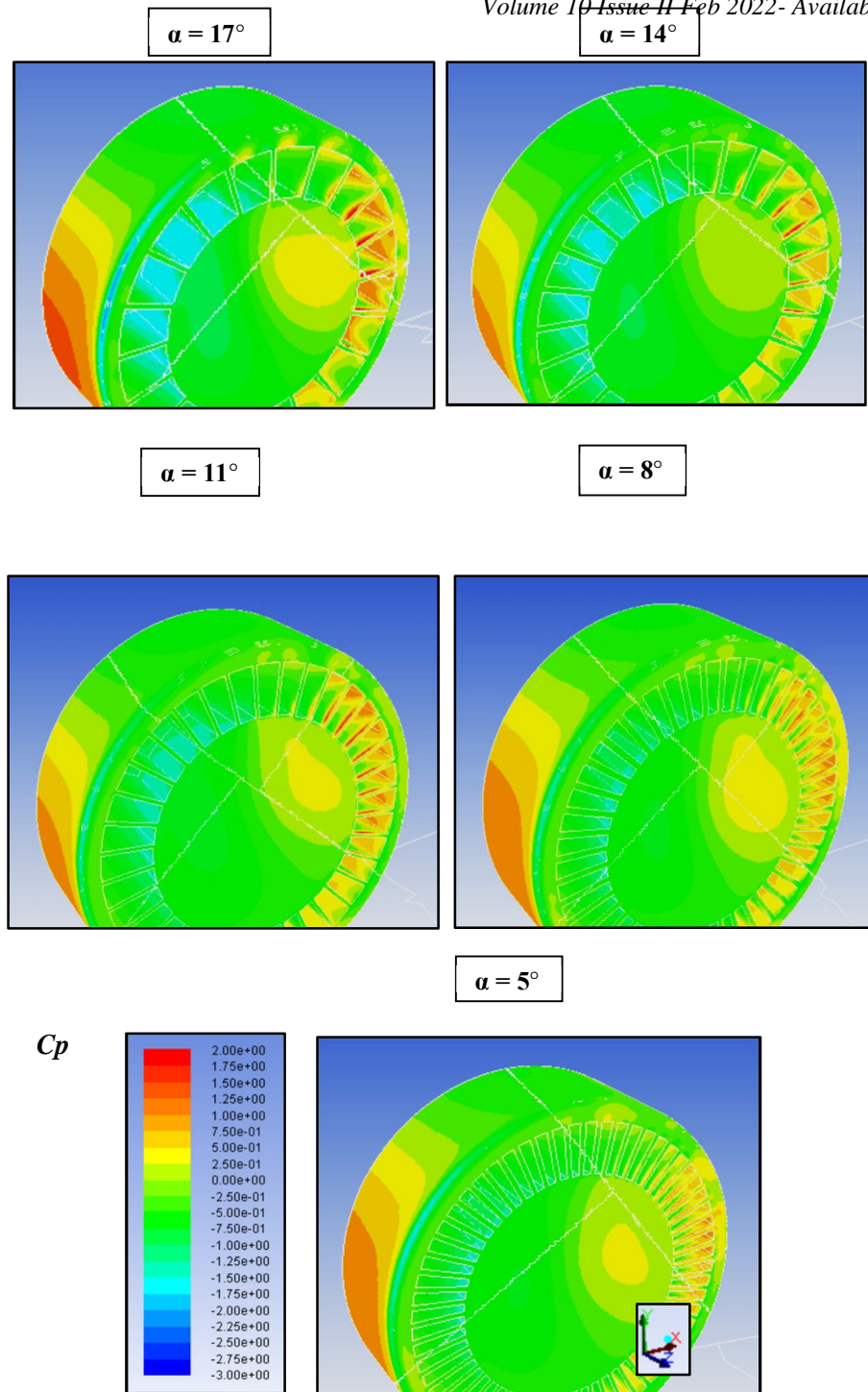
Figure 14. Coefficient of pressure contours at the wheel side at various spokes angles (α) for NPT wheel models.

VII. CONCLUSION

The adopted RNG k- ε turbulence model for the steady-RANS solution with utilizing non-equilibrium wall function approach almost matching the experimental pressure profile of the ST wheel except for the inaccuracy in obtaining the localized pressure spikes. The MRF model showed a near-identical flow characteristic, which is a good approach for simulating the realistic effect of wheel rotation. The distinct shifting in the stagnation and separation angles due to wheel rotation is precisely captured. Furthermore, this model developed a reasonable flow physics over the NPT wheel case study with a harmonic convergence attitude. In conclusion,

the NPT wheel, compared to the ST, has a dramatic increase in drag force by approximately 31% and a slight increase in the lift force.

The NPT side pressure profile variations were the most dominant in influencing the aerodynamic coefficients, where tremendous fluctuations are monitored. Furthermore, the NPT resistive moment value was – 0.33 while it just reached – 0.031 for the ST wheel case. That is extremely high that using NPT wheels can increase the typical rolling resistance by three doubles at a vehicle speed of 100 Km/h.

A shape-optimization process on minimizing the spokes spacing angle (α) of the NPT wheel is carried out over five different angles. The circumferential pressure profile shows marginal differences for various spacing angles. As the spacing angle decreases, the pressure amplitude and ΔCp gradually reduce, especially at the critical region, consequently, lowers the drag force and moment and raising lift force. In conclusion, the minimized spokes angle benefits drag reduction, while the applied resistive moment is still relatively high. After all, at wheel side profile is a critical factor from the aerodynamic perspective, and its shape-optimization demands sincere efforts and more attention.

VIII. ACKNOWLEDGEMENT

REFERANCES

[1] Morelli A. Aerodynamic actions on an automobile wheel. In Proceedings of the Symposium on Road Vehicle Aerodynamics. City University, London 1969 Nov.

[2] Stapleford WR, Carr GW. Aerodynamic characteristics of exposed rotating wheels. Motor Industry Research Association; 1969.

[3] Cogotti A. Aerodynamic characteristics of car wheel. Int. J. of Vehicle Design. 1983.

[4] Fackrell JE. The aerodynamics of an isolated wheel rotating in contact with the ground.

[5] Knowles RD, Saddington AJ, Knowles K. On the near wake of a Formula One front wheel. Proceedings of the Institution of Mechanical Engineers, Part D: Journal of Automobile Engineering. 2013 Nov;227(11):1491-502.

[6] Mears AP, Crossland SC, Dominy RG. An investigation into the flow-field about an exposed racing wheel. SAE Technical Paper; 2004 Mar 8.

[7] Van den Berg MA. Aerodynamic interaction of an inverted wing with a rotating wheel (Doctoral dissertation, University of Southampton).

[8] Heyder-Bruckner J. The aerodynamics of an inverted wing and a rotating wheel in ground effect (Doctoral dissertation, University of Southampton).

[9] Sprot AJ, Sims-Williams DB, Dominy RG. The aerodynamic characteristics of a fully deformable Formula One wind tunnel tyre. SAE International journal of passenger cars. Mechanical systems.. 2012 Apr 16;5(2):1026-41.

[10] Croner E, Bézard H, Sicot C, Mothay G. Aerodynamic characterization of the wake of an isolated rolling wheel. International journal of heat and fluid flow. 2013 Oct 1;43:233-43.

[11] Haag L, Blacha T, Indinger T. Experimental investigation on the aerodynamics of isolated rotating wheels and evaluation of wheel rotation models using unsteady CFD. International Journal of Automotive Engineering. 2017;8(1):7-14.

[12] Rajaratnam E, Walker D. Experimental and computational study of the flow around a stationary and rotating isolated wheel and the influence of a moving ground plane. SAE Technical Paper; 2019 Apr 2.

[13] Yu X, Jia Q, Bao D, Yang Z. A comparative study of different wheel rotating simulation methods in automotive aerodynamics. SAE Technical Paper; 2018 Apr 3.

[14] Hobeika T, Sebben S. CFD investigation on wheel rotation modelling. Journal of Wind Engineering and Industrial Aerodynamics. 2018 Mar 1;174:241-51.

[15] Lewis R, Cross M, Ludlow D. The influence of rotating wheels on the external aerodynamic performance of a vehicle. InThe International Vehicle Aerodynamics Conference 2014 Nov 12 (pp. 161-173). Woodhead Publishing.

[16] Heo H, Ju J, Kim DM, Rhie S. A study on the aerodynamic drag of a non-pneumatic tire. InInternational Design Engineering Technical Conferences and Computers and Information in Engineering Conference 2012 Aug 12 (Vol. 45059, pp. 517-521). American Society of Mechanical Engineers.

[17] Heo H, Ju J, Kim DM, Kim H. A computational study of the flow around an isolated non-pneumatic tire. SAE International Journal of Passenger Cars-Mechanical Systems. 2014 May 10;7(2014-01-9123):405-12.

[18] Li H, Xu Y, Si C, Yang Y. A research on aerodynamic characteristics of non-pneumatic tire. Mechanics & Industry. 2021;22:27.

[19] Bhatia D, KR P, Ponangi BR, Athadkar M, Dsouza CV. CFD study of aerodynamic performance of non-pneumatic tyre with hexagonal spokes. Proceedings of the Institution of Mechanical Engineers, Part D: Journal of Automobile Engineering. 2021 May 3:09544070211013124.

[20] Soliman MZ, El-Baz AR, Abdel-Aziz MA, Abdel-Aziz N, Sugar-Gabor O. Numerical investigation of the effect of tread pattern on rotating wheel aerodynamics. International Journal of Automotive and Mechanical Engineering. 2020;17(4):8234-45.

[21] Fluent IN. FLUENT 6.3 user's guide. Fluent documentation. 2006 Nov.

INTERNATIONAL JOURNAL
FOR RESEARCH

IN APPLIED SCIENCE & ENGINEERING TECHNOLOGY

Call : 08813907089 ◯ (24*7 Support on Whatsapp)